

Coating of Polypropylene Non-Woven Fabric with Layered Double Hydroxides Bearing Antioxidant and Antibacterial Natural Compounds

Francesca Cicogna, Elisa Passaglia, Elyazid Elainaoui, Emilia Bramanti, Werner Oberhauser, Beatrice Casini, Benedetta Tuvo, Maria-Beatrice Coltelli, Luca Panariello, and Serena Coiai*

Layered double hydroxides (LDHs) containing immobilized rosmarinic acid or eugenol have been employed to functionalize polypropylene (PP) non-woven fabric (NWF), commonly used to manufacture protective clothing such as surgical masks. Rosmarinic acid and eugenol have recognized biological activities, such as antimicrobial, antioxidant, and anti-inflammatory capabilities, and they have been employed in this work both as synthetic, commercial compounds and as raw mixtures extracted from agri-food matrices. These encapsulated hybrid systems have been designed to gradually release the active molecules while protecting them from degradation processes caused by light and heat. Two different NWF modification strategies have been employed to increase the adhesion capacity of the hybrids: cold plasma treatment with oxygen and polydopamine coating. Both methodologies have increased the amount of hybrid deposited on the NWF surfaces, giving significant resistance to thermo-oxidation, the controlled migratory capacity of active molecules, and, in the case of the eugenol-containing system, significant bactericidal activity against *Staphylococcus aureus*.

is PP non-woven fabric (NWF), which exhibits outstanding overall thermal and mechanical performance and superior filtering capabilities.^[2] Given its exceptional properties, PP NWF is used in various applications, including manufacturing personal protective equipment like surgical masks. The enhancement of the functionality of PP NWF in face masks to protect against viruses and bacteria has become crucial mostly in the COVID-19 pandemic. One effective strategy has been to coat the PP NWF with antimicrobial and antioxidant substances, thus significantly improving its protective properties.^[3–6]


Natural bioactive compounds are becoming increasingly popular to replace synthetic functional agents.^[7,8] Among them, phenolic compounds possess attractive antioxidant, antibacterial, antiviral, and anti-inflammatory properties.^[9,10] They are minimally or non-toxic at reasonable doses, and they can be potential byproducts of the agri-food industry's processing.^[11]

Polymers can be modified with polyphenols, resulting in various advantageous properties. For example, phenolic compounds have been incorporated in poly(vinyl alcohol) for food packaging applications, getting an effective thermal stabilization of the composite films and inhibition of *Listeria innocua*

1. Introduction

Polypropylene (PP) is a highly versatile and widely used polymer with exceptional mechanical, thermal, and chemical properties.^[1] One of the most notable products derived from PP

F. Cicogna, E. Passaglia, E. Elainaoui, E. Bramanti, S. Coiai
 National Research Council
 Institute for the Chemistry of OrganoMetallic Compounds (CNR-ICCOM)
 SS Pisa, Via Moruzzi 1, Pisa 56124, Italy
 E-mail: serena.coiai@pi.iccom.cnr.it

 The ORCID identification number(s) for the author(s) of this article can be found under <https://doi.org/10.1002/macp.202300148>

© 2023 The Authors. Macromolecular Chemistry and Physics published by Wiley-VCH GmbH. This is an open access article under the terms of the Creative Commons Attribution-NonCommercial-NoDerivs License, which permits use and distribution in any medium, provided the original work is properly cited, the use is non-commercial and no modifications or adaptations are made.

DOI: 10.1002/macp.202300148

W. Oberhauser
 National Research Council
 Institute for the Chemistry of OrganoMetallic Compounds (CNR-ICCOM)
 Via Madonna del Piano 10, Sesto Fiorentino (FI) 50019, Italy
 B. Casini, B. Tuvo
 Department of Translational Research and the New Technologies in
 Medicine and Surgery
 University of Pisa
 Pisa 56123, Italy
 M.-B. Coltelli, L. Panariello
 Department of Civil and Industrial Engineering
 University of Pisa
 Largo L. Lazzarino 1, Pisa 56122, Italy

growth.^[12,13] PP has been extruded with grape extract displaying both antioxidant characteristics and antimicrobial activity against Gram-negative (*Escherichia coli*) and Gram-positive (*Bacillus subtilis*) bacteria.^[14,15] In addition, our research group has recently deposited clove, olive leaf, and green tea extracts onto PP NWF, demonstrating a reduction of the viral load exceeding 90% against *Human Adenovirus* type 5 (HAdV5) and ranging from 30% to 90% against *Human Coronavirus* 229E (HCoV229E).^[16]

There are several strategies to integrate active compounds within a polymeric material, including films, electrospun fibers, and self-assembled coatings.^[8] The traditional blending of polyphenols with polymeric materials followed by extrusion or solution casting, for instance, results in active films based on additives migration, which release the active components by diffusion and adsorption. Importantly, this mechanism implies time-limited antioxidant/antimicrobial protection, as polyphenols are depleted from the material very fast. The melt blending of polyphenols with the polymer matrix may also encounter several drawbacks, such as the thermal instability of polyphenols at the polymer processing temperatures (generally above 180 °C),^[17] the possible change in the optical, thermal, and mechanical properties of the polymer matrix, and the poor affinity of polyphenols with apolar polymer matrices such as PP, which may generate non-homogeneous distribution and leaching effects.^[14]

Depositing active substances on a surface can overcome some of the limitations associated with blended bulk materials while preserving the properties of the polymer matrix and the active components. However, in the case of inert polymers like polyolefins, it is fundamental to activate the surface's material to increase the polymer hydrophilicity and wettability. This step is crucial to establish the interactions with polyphenols and, thus, to enable their tunable migration.

Cold plasma activation is a commonly used technique for improving adhesion to inert substrates. It is versatile, safe, and inexpensive. It is environmentally friendly since it does not use solvents or chemical reagents and, in the presence of oxygen, it works by generating functional groups like carboxyl and carbonyl groups on the polymer surface.^[18–20] It has been demonstrated that plasma treatment modifies surface features with low impacts on the bulk properties of PP films or PP NWF.^[21] Recent studies have shown that plasma activation can effectively improve the adhesion of active substances to polymer surfaces, such as linear low-density polyethylene and PP. For example, plasma treatment has been found to enhance the attachment of onion and potato peel extracts or ascorbic acid to these surfaces.^{[22],[23]} Our group has recently demonstrated that plasma treatment of PP NWF can enhance the immobilization of natural extracts on the activated surface of NWF.^[24]

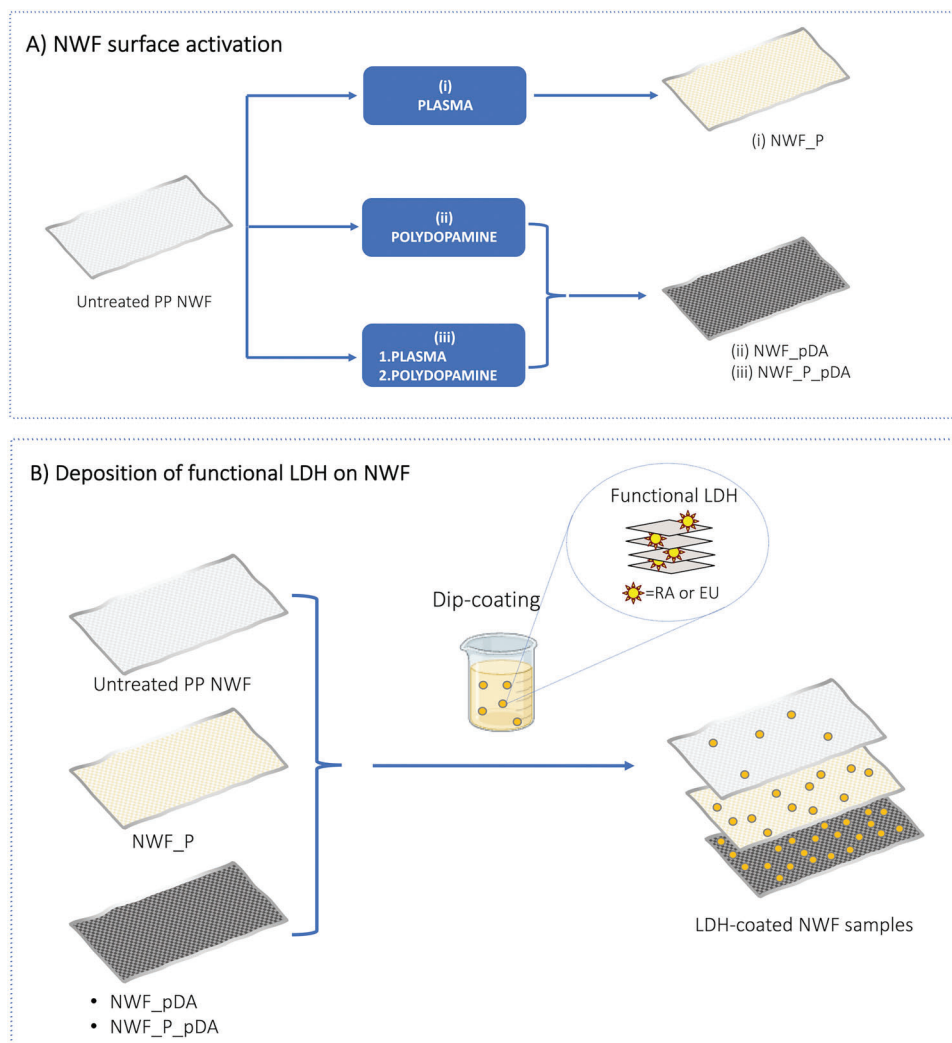
Polydopamine (pDA) is a biologically inspired polymer with strong adhesive properties, and it can adhere to many substrates, including PP-based surfaces. PDA is produced in situ by dopamine oxidative self-polymerization in buffered water, without damaging the surface and giving a stable, thin coating layer with excellent adsorption capabilities.^[25] PDA is biocompatible, thermally stable, and has antioxidant and antimicrobial properties.^[26] Furthermore, the functional groups of pDA (quinone, catechol, carboxyl, amine, imine, and phenolic groups) can react with a wide range of functionalities, making it versatile.^[27] Researchers have used pDA to modify PP meshes

with antibacterial drugs,^[28] and to create chemically resistant surfaces by coating PP chips and centrifuge tubes with pDA and a thin film of layered double hydroxides (LDHs).^[29] Furthermore, plasma activation before dopamine polymerization can enhance the thickness of pDA layers on polymeric substrates.^[28,30]

Although polyphenols have antioxidant and antimicrobial features, they are often susceptible to thermal and photochemical instability, and, additionally, to fully benefit from their properties, their gradual release over time is crucial and must be controlled. The immobilization of these molecules in suitable host-guest systems can overcome both requests. Indeed, several inorganic nanocarriers can encapsulate and protect bioactive compounds while modulating their release properties.^[31,32] Among these, LDHs have been proven to be particularly effective. LDHs are widely used in pharmaceuticals, cosmetics, and nutraceuticals for encapsulating active ingredients due to their ability to intercalate and adsorb various organic anions, which can be released in a controllable manner.^[33,34] Intercalation protects bioactive molecules from thermal and photochemical degradation, increases their solubility in water, and in some cases, increases their bioavailability. The literature reports numerous examples of intercalation of phenolic acids, like caffeic acid, ferulic acid, and rosmarinic acid, in LDHs.^[35–39] Our research group has recently intercalated rosmarinic acid between the lamellae of an Mg-Al LDH.^[38,39] The effective dispersion of a hybrid system in polymer matrices allows a controlled release of the active molecule, and the composite materials have exhibited antimicrobial and antioxidant activities. LDHs have been also used to encapsulate neutral molecules, such as natural curcuminoids.^[40] Thermogravimetric analysis (TGA) and UV exposure data have indicated that the curcuminoids were stabilized within the matrix. The resulting hybrids have exhibited a slow and sustained release of curcuminoids in acidic environments and have demonstrated activity against bacteria and fungi. Furthermore, LDHs have been utilized to confine neutral polyphenols found in olive mill wastewater.^[41,42] The resulting hybrid system has been used as a functional additive for both PP and poly(butylene succinate), achieving significant antioxidant and antibacterial activity.

In this work, we describe the preparation of host-guest hybrid systems by immobilizing rosmarinic acid (RA-H) and eugenol (EU), two natural polyphenols with antioxidant and antimicrobial properties,^[43–45] in LDHs to protect the organic molecules and promote their controlled release. Both synthetic RA-H and EU, and the extracts of sage and clove buds naturally containing the same polyphenols have been used to modify the LDHs. The resulting hybrid systems have been compared with respect to their structural, thermal, and functional properties. To deposit the hybrid particles on PP NWF used in surgical masks, the fabric was dip-coated after i) plasma pretreatment, ii) pDA coating, and iii) both treatments to enhance their adhesion capability (Scheme 1).

All the samples have been characterized by Fourier Transform Infrared spectroscopy (FTIR), scanning electron microscopy (SEM), and TGA to confirm the effective coating with the hybrid particles. The materials' thermal oxidation resistance has been assessed by measuring the oxidation induction time (OIT) via differential scanning calorimetry (DSC), and their antimicrobial capacity has been evaluated in vitro against *Pseudomonas aerugi-*



Scheme 1. Process of NWF modification: a) The surface activation using plasma, pDA, or a combination of both methods in sequence; b) the subsequent deposition of functional LDHs through dip-coating.

nosa and *Staphylococcus aureus*. The kinetics of migration of the various LDH-coated substrates in alcohol solutions has also been preliminarily investigated.

2. Results and Discussion

2.1. Preparation and Characterization of Rosmarinic Acid and Eugenol Modified LDH-hybrid Systems

Solutions containing RA-H and EU were obtained by macerating *Salvia officinalis* leaves and clove buds in ethanol, respectively. UV-vis spectra of the extracts were comparable to those of commercial RA-H and EU, as shown in **Figure 1**. The quantitation of RA-H and EU in the extracts was estimated by using calibration curves at 329 and 282 nm, respectively, of standard solutions of RA-H and EU (Figure S1, Supporting Information), and by interpolating the absorbance values of the extracts at 329 and 282 nm. The concentration of RA-H and EU in the extracts was found to be 2.9 and 15 mg mL⁻¹, respectively. This corresponds to 2 wt.%

of RA-H compared to dried sage leaves and 15 wt.% by weight compared to dried cloves (as detailed in the Experimental Section).

Both pure commercial molecules and the extracts were used for LDH modification.

First, modified LDHs were produced using synthetic RA-H and sage extract (LDH-RA_{syn} and LDH-RA_{ext}) through anion exchange of LDH-NO₃ under specific pH conditions (see Experimental Section). This procedure was previously optimized for LDH-RA_{syn} and gave favorable results both in terms of the intercalation of the carboxylate anion (RA) and the amount of immobilized organic molecule.^[38,39] The hybrid products shared similar chemical and structural characteristics, as confirmed by FTIR spectra, which showed the typical vibration modes of pristine LDH and new absorption bands assigned to RA, like the bands at 1590 and 1384 cm⁻¹ (Figure S2, Supporting Information). We observed a selective immobilization of RA from sage extract, and X-ray diffraction analysis (XRD) revealed that RA was intercalated between the lamellae in both cases, resulting in an increase in

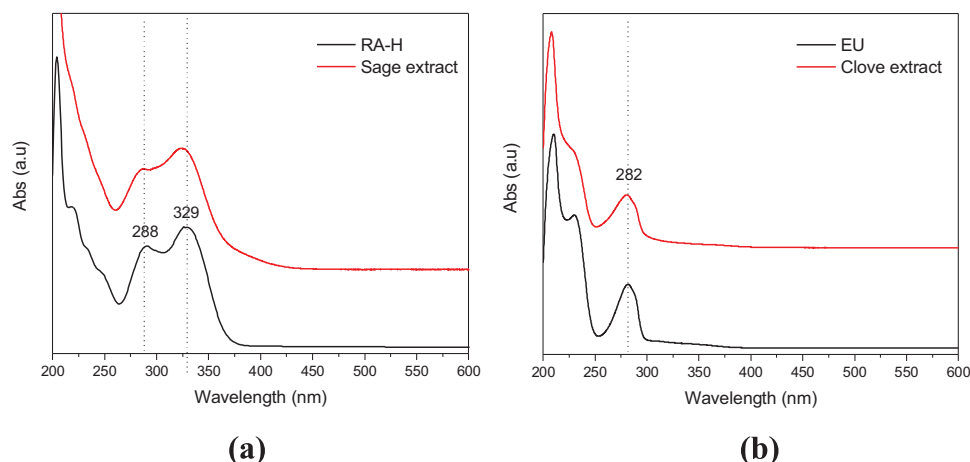


Figure 1. UV-vis spectra of a RA-H standard solution and sage extract a) and EU standard solution and clove bud extract b). The spectra have been vertically translated for a better comparison.

Table 1. Summary of modified LDHs features: polyphenol type and content, (003) XRD diffraction peak, and corresponding basal spacing $d(003)$.

Sample	Functional molecule	RA content (wt.%) ^{a)}	EU content (wt.%) ^{a)}	2θ (°)	$d(003)$ (nm)
LDH-RA _{syn}		43.5	–	3.9	2.26
LDH-RA _{ext}		35.9	–	3.9	2.26
LDH-EU _{syn}		–	21.7	11.6	0.90
LDH-EU _{ext}		–	29.3	5.0	1.76

^{a)} The RA and EU content was determined by UV-vis analysis based on the calibration curves of commercial standard solutions (Figure S1, Supporting Information).

basal distance $d(003)$ from 0.90 to 2.26 nm (Table 1 and Figure S3, Supporting Information).

According to UV-vis analysis, the amount of RA immobilized on LDH-RA_{syn} and LDH-RA_{ext} was 43 wt.% and 36 wt.%, respectively (Table 1). The thermal stability of both products was also investigated (Figure S4, Supporting Information). The TGA thermograms of the hybrids were similar and showed the water loss steps, the dehydroxylation of the lamellae, and a weight loss between 220 and 260 °C. The last weight loss corresponds to the desorption and initial decomposition of the organic anions, in accordance with the literature,^[38,39] confirming the stability of these hybrid systems up to about 260 °C. All the data on LDH-RA_{syn} and LDH-RA_{ext} consistently suggest that synthetic commercial RA-H as well as RA-H contained in the raw extract of aromatic plants can be successfully intercalated in LDH without purification, resulting in a viable, sustainable alternative for preparing LDH hybrids.

Similarly, we prepared the hybrid system based on EU and LDH using both synthetically derived EU and clove bud extract (LDH-EU_{syn} and LDH-EU_{ext}). In this case, we used the LDH calcination and regeneration method, which takes advantage of the high adsorption capacity exhibited by LDH lamellae during the regeneration step.^[46] FTIR spectra of the synthesized products confirmed the successful synthesis of the hybrid products, showing the characteristic absorption bands of EU (Figure 2). In particular, the hybrids showed the OH stretching of the phenolic group in the range 3000–3700 cm^{-1} , the symmetric and asym-

metric stretching of the CH_2 and CH_3 groups in the area between 2940 and 2850 cm^{-1} , the absorptions at 1512, 1610, and 1630 cm^{-1} typical of the aromatic ring, the bending of the CH_2 and CH_3 groups from 1450 to 1350 cm^{-1} , and the signals at

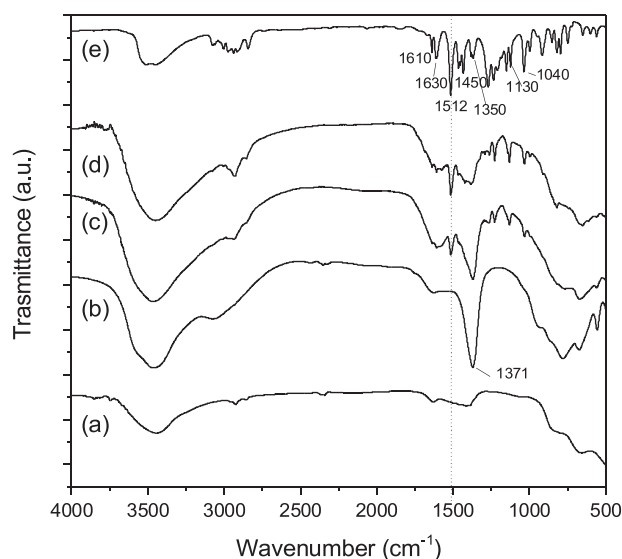


Figure 2. FTIR spectra of calcinated-LDH a), LDH-CO₃ b), LDH-EU_{syn} c), LDH-EU_{ext} d), and EU e).

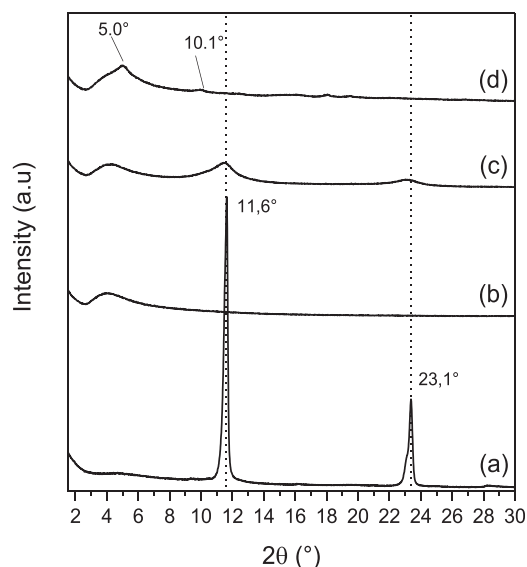


Figure 3. XRD patterns of LDH-CO₃ a), calcinated-LDH b), LDH-EUsyn c), and LDH-EUext d).

1130 and 1040 cm⁻¹ due to the stretching of the C-O and C-O-C groups. The intensity of EU vibrational signals was noticeably higher in LDH-EUext compared to LDH-EUsyn, in agreement with the greater EU content determined through UV-vis analysis. The amount of EU immobilized on LDH-EUsyn and LDH-EUext was indeed 21.7 wt.% and 29.3 wt.%, respectively (Table 1). Additionally, in the LDH-EUsyn spectrum, a relatively broad band at around 1370 cm⁻¹, characteristic of LDH-CO₃, is clearly visible. This absorption band is due to carbonate anions that have been likely reintegrated into the lamellar structure during the regeneration phase.^[47]

According to the presence of carbonate anions observed by FTIR analysis, the XRD pattern of the LDH-EUsyn sample revealed diffraction peaks at 11.6 and 23.1° (2θ), which corresponded to the (003) and (009) reflections of LDH-CO₃, respectively, indicating the recovery of the original LDH phase after reconstruction (Figure 3). This result suggested that EU was not incorporated into the interlamellar space of LDH-EUsyn. Instead, it appears that carbonate anions have occupied the interlamellar space, balancing the positive charge and giving a layered structure, which is responsible for the previously discussed diffraction signals. Furthermore, reduced crystallinity (broad peaks) was observed, which was likely due to the partial disorder and reorganization of the LDH lattice during the reconstruction process.^[37] On the other hand, the LDH-EUext hybrid did not show the recovery signals of the original LDH phase but a broad reflection with a maximum at approximately 5°, a weak signal at 10.1°, and a few other low intense reflexes at higher 2θ values. The structure appeared disordered, but assuming that the diffraction angle at 5° may be associated with the (003) reflection due to intercalation of EU or of other organic compounds present in the extract, and that the signal at 10.1° is due to higher-order diffraction (006), we can calculate the corresponding interlamellar distance of 1.76 nm, which is rational for an EU intercalation, considering mainly its size.^[48] The clove extract has EU as the main polyphenol with traces of other molecules.^[16,49] It is not

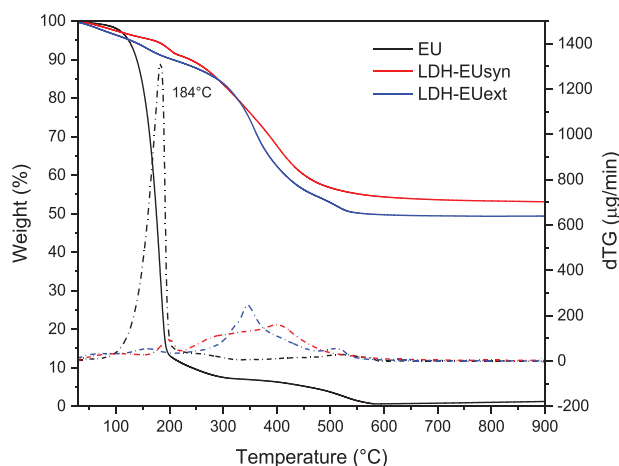


Figure 4. TG and dTG curves of LDH-EUsyn, LDH-EUext, and EU.

possible to establish with certainty whether EU has been intercalated into the LDH-EUext system; it can be hypothesized that the different chemical environment in which LDH-EUext and LDH-EUsyn were obtained, through the regeneration of calcined LDH, led to the formation of two distinct crystallographic structures.

Figure 4 shows the TG curves and the corresponding first derivatives (dTG curves) of EU and LDH-EU hybrids. EU showed a weight loss of 99% between 30 and 900 °C, with the maximum degradation rate occurring at 184 °C. The LDH-EUsyn and LDH-EUext hybrids have similar curves with a two-stage weight loss pattern between 30–150 °C and 150–600 °C, respectively. The first step was attributed to the loss of the water adsorbed at the surface or between layers, while the second step was due to the thermal decomposition of immobilized EU, whose presence was confirmed by FTIR, along with the dehydroxylation of the LDH lattice and the decomposition of other anions within the structure. The differences observed in the thermograms of LDH-EUsyn and LDH-EUext within the temperature range of 150 to 600 °C can be attributed to the degradation of carbonate anions found in LDH-EUsyn. This observation is supported by a comparison with the thermogram of LDH-CO₃ (Figure S5, Supporting Information) and is in accordance with the findings previously discussed regarding XRD and FTIR results. Although it is unclear where exactly the thermal decomposition of the EU moiety occurs, it is noteworthy that the decomposition temperatures of LDH-EUsyn and LDH-EUext are higher than those of EU alone. Therefore, it can be concluded that the EU in the hybrids has been protected from the inorganic fraction, gaining thermal stability.

The antioxidant activity of RA-H, EU, LDH-RA, and LDH-EU hybrids was assessed by measuring their ability to scavenge the stable 2,2-diphenyl-1-picrylhydrazyl (DPPH) free radical.^[50,51] To compare the antioxidant capacity of modified LDHs to that of free molecules, solutions of free polyphenols and LDH suspensions with the same active ingredient concentration were prepared and then comparatively tested. The antioxidant activity of the samples was determined based on the percentage of quenched DPPH after 30 min and 24 h, as described in the Experimental Section, (Table 2).

The data collected revealed that EU has a lower antioxidant activity compared to RA-H, as the percentage of quenched DPPH

Table 2. Percentage of quenched DPPH after 30 min and 24 h in the presence of RA-H, EU, and modified LDHs.

Sample	% DPPH quenched at different times ^{a)}	
	30 min	24 h
RA-H	67 ± 9	76 ± 5
EU	13 ± 3	69 ± 2
LDH-RA _{syn}	4.8 ± 0.4	30 ± 6
LDH-RA _{ext}	1.7 ± 0.4	18 ± 6
LDH-EU _{syn}	0.7 ± 0.2	13 ± 1
LDH-EU _{ext}	2.4 ± 0.2	13 ± 4

^{a)} Data are reported as the mean of triplicate measurements ± standard deviation (SD) (n = 3).

was lower for EU than for RA-H after 30 min. However, after 24 h, although the percentage of DPPH that reacted with EU was still lower than that of RA-H, the difference between the two values remarkably decreased, indicating a good antioxidant capacity for both molecules. Furthermore, the antioxidant activity of the modified LDHs was found to be lower than that of free molecules, possibly due to the lower number of molecules released into the suspension during the reaction period and, thus, available for the reaction with DPPH. One of the significant advantages of creating host-guest systems with intercalated active molecules is, indeed, the controlled release of the active molecule, which prolongs its functional activity over time. Nevertheless, rosmarinate anions trapped between the LDH layers still retained their anti-radical power, albeit with slower kinetics. This may be attributed to the time required for the guest to diffuse from the interlayer region of LDH-RA hybrids into the solution. Similar results were observed with LDH-EU hybrids, despite EU, in contrast to RA-H does not form ionic bonds with the inorganic lamellae.

2.2. Preparation and Characterization of Plasma and Polidopamine Modified PP Non-Woven Fabrics

PP NWF surface activation was induced by cold plasma in the presence of oxygen or obtained by pDA coating. These two meth-

ods are complementary because they have different characteristics, as previously described. Both activation processes add functional groups that can interact with functional LDHs. The oxygen-containing groups generated by plasma treatment are polar and hydrophilic, allowing for positive interactions with functional LDHs. On the other hand, the catechol present on the surface of NWF after pDA coating can coordinate and immobilize metal ions of LDHs.^[29] Therefore, the increased interactions between the activated PP surface and functional LDHs can increase the load and quantity of immobilized functional LDHs.

We worked out our approach to activate the PP NWF surface, which involved three different procedures: cold oxygen plasma i), pDA coating ii), and a combination of these treatments in sequence iii) (Scheme 1a). PP NWF was taken from the outer layer of face masks, which is potentially exposed to a higher concentration of viruses and bacteria, thus leaving unchanged the inner layer of the face mask, which is in direct contact with the skin.

Figure 5 shows the ATR FTIR spectrum of plasma-treated PP NWF (NWF_P). A new band envelope in the region between 1800 and 1500 cm⁻¹ with a maximum at 1715 cm⁻¹ was observed, which can be attributed to the presence of oxidized species formed on the PP surface due to plasma treatment.^[24] By performing a deconvolution procedure in the range 1850–1500 cm⁻¹ (Figure 5b), four main contributions to the envelope were identified^[24]: the band at 1740 cm⁻¹ associated with C=O stretching of peroxyacid, carboxylic acid monomer and possibly esters (also unsaturated), the band at 1710 cm⁻¹ due to C=O stretching of carboxylic acid dimer or aldehydes, ketones, and possibly esters, the band at about 1647 cm⁻¹ due to unsaturated carbonyls (both aldehydes and ketones) and vinyl double bonds, and the band at about 1590 cm⁻¹ probably due to the bending of -NH and -NH₂ groups generated by the reaction of carbon radicals with nitrogen when the treated samples are exposed to air.

The pDA coating was performed on both pristine NWF and NWF_P. The ATR FTIR spectra of PP NWF (NWF), PP NWF coated with pDA (NWF_pDA), and PP NWF plasma-activated and pDA coated (NWF_P_pDA) revealed the appearance of new bands at about 3140 cm⁻¹ and in the range between 1500 and 1200 cm⁻¹ in NWF_pDA and NWF_P_pDA, which overlap with some typical PP bands (**Figure 6**). Upon comparison with the spectra of pDA and dopamine (Figure S6, Supporting

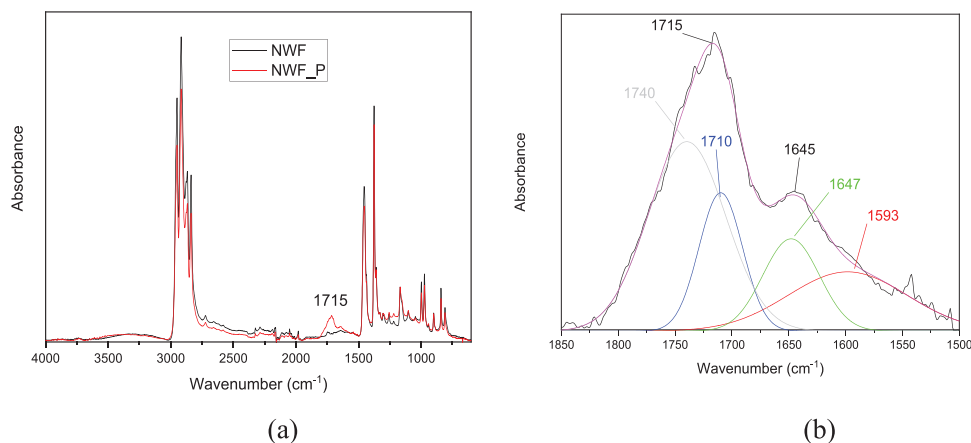


Figure 5. ATR FTIR spectra of NWF and NWF_P a); deconvolution of the spectral region between 1850 and 1500 cm⁻¹ of NWF_P b).

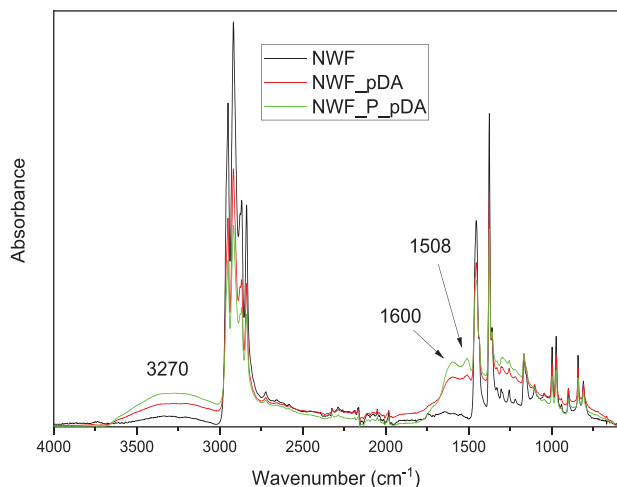


Figure 6. ATR FTIR spectra of NWF, NWF_pDA, and NWF_P_pDA. Spectra were normalized with respect to the PP band at 1167 cm^{-1} .

Information),^[52] the band at 3270 cm^{-1} was found to be associated with the O-H stretching of catechol and with the amine stretching of pDA. Moreover, the bands at 1600 and 1508 cm^{-1} confirmed the formation of aromatic amine (indole) during dopamine polymerization, associated with C=C and C=N stretching, respectively. Notably, when the spectra were normalized with respect to the band at 1167 cm^{-1} (CH_3 rocking vibration of PP), the bands characteristic of pDA in the NWF_P_pDA were more intense than in NWF_pDA sample, confirming that the plasma activation followed by pDA coating led to a higher pDA content.

SEM analysis of NWF, NWF_P, and NWF_pDA (**Figure 7**) showed that NWF is composed of fibers with a smooth surface and a regular diameter of approximately $10\text{--}20\text{ }\mu\text{m}$. Melted zones, which are regularly distributed on the surface of NWF and play a crucial role in bonding the fibers and conferring mechanical strength to the material, are also visible (**Figure 7a1**). Upon plasma treatment (**Figure 7b1-b3**), some defects, scratches, and etching were observed on the surface of the melt area and fibers.

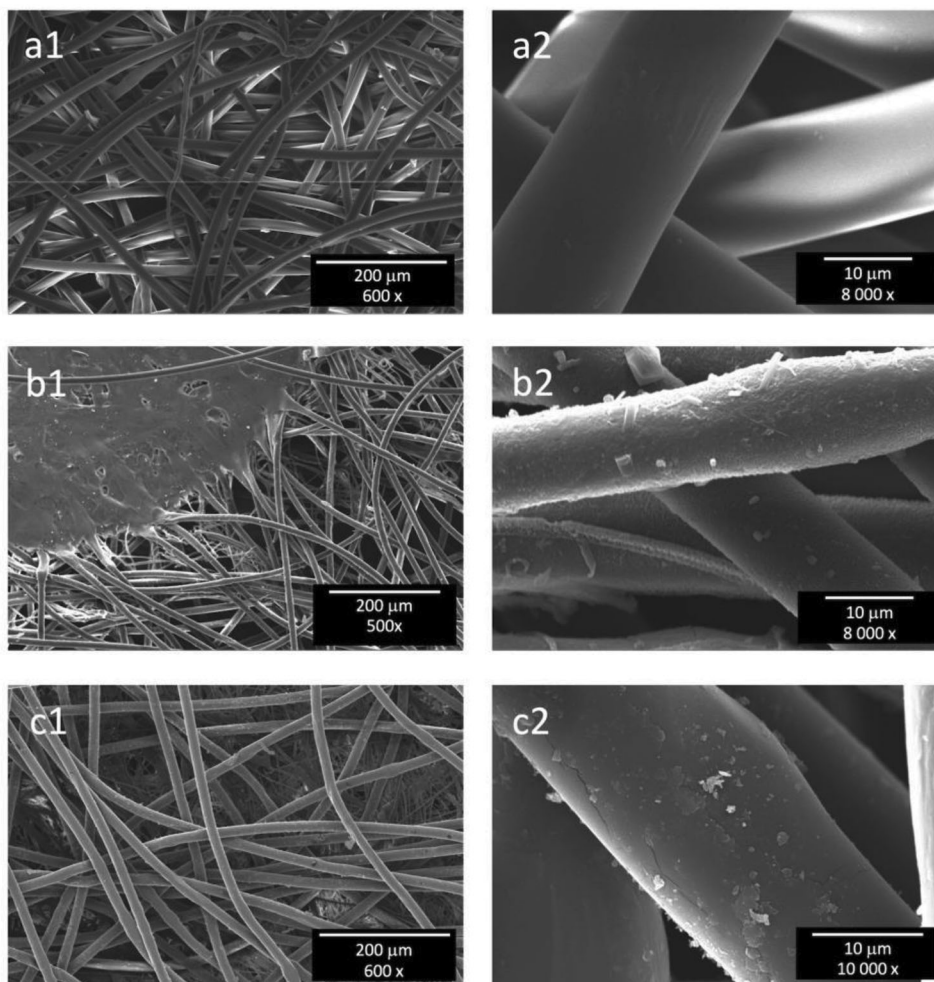


Figure 7. SEM micrographs at different magnification of NWF a1, a2); NWF_P b1, b2), and NWF_pDA c1, c2).

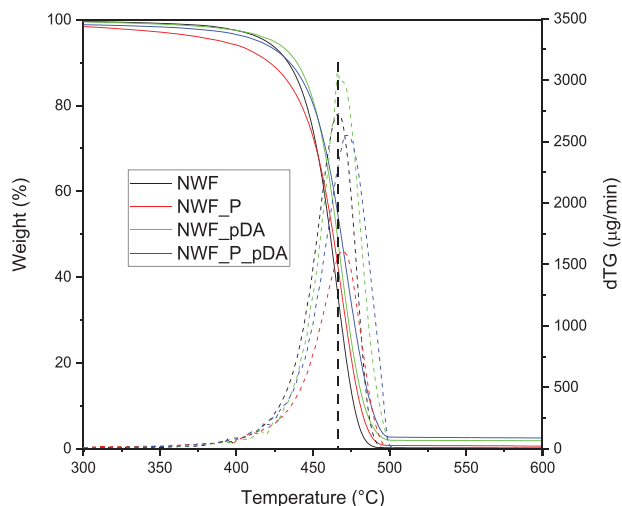


Figure 8. TGA and dTG curves of NWF, NWF_P, NWF_pDA, and NWF_P_pDA between 300 and 600 °C.

The ion bombardment during plasma treatment and the formation of oxidized species may cause damage to the fiber surface, resulting in a rough surface. In the case of NWF_pDA, the SEM micrographs showed that the application of pDA created a thin layer on the fibers, which appeared less smooth than those of pure NWF. The surface of the fibers also exhibited some wrinkles and small particles. The observed micro-aggregates may be due either to the polymerization of dopamine on the fibers or the adhesion of pDA formed in the solution.

Figure 8 and **Table 3** show TGA data of NWF, NWF_P, NWF_pDA, and NWF_P_pDA. The results revealed that the degradation of all samples occurred in a single step, which was attributed to the PP decomposition. Plasma activation reduced the thermal stability of PP, as evidenced by the lower $T_{5\%}$ (the temperature at which the sample lost 5 wt.%) of NWF_P compared to NWF. This behavior is attributed to the presence of oxidized groups on the NWF_P surface thereby accelerating the beginning of polymer decomposition. The coating of pDA on NWF in the

NWF_pDA sample increased the $T_{5\%}$ of NWF by approximately 3 °C. This temperature increase is likely due to the thin layer of pDA protecting the PP fibers from decomposition during the initial stages of thermal treatment. However, in the NWF_P_pDA sample, the $T_{5\%}$ was like that of NWF, suggesting that pDA only partially compensated for the thermal instability of the surface-oxidized PP.

The temperature corresponding to the maximum decomposition rate (T_{inf}) was similar for all samples, indicating that plasma activation and pDA coating only affected the thermal decomposition of PP fibers during the initial stages and did not impact bulk properties. The residual mass of NWF and NWF_P was lower than that of NWF_pDA and NWF_P_pDA (i.e., the latter were covered with pDA), whose pyrolysis produced a remarkable amount of carbon char (approximately 54 wt.%)^[53,54] (Figure S7, Supporting Information). Based on this data, 1.7 and 3.5 wt.%, of pDA was estimated in NWF_pDA and NWF_P_pDA, respectively.

2.3. Deposition of Functional LDHs on PP Non-Woven Fabrics

Neat NWF and modified NWFs were coated with functional LDHs. To carry out the tests we used LDH-RASyn and LDH-EUSyn and, for the sake of simplicity, we will refer to these hybrids as LDH-RA and LDH-EU, respectively.

All NWFs were immersed in an aqueous suspension of LDH, dried, and analyzed (Scheme 1b). Upon comparing the ATR FTIR spectra of pure NWFs and LDH-coated NWFs (**Figure 9**), several characteristic absorption bands were observed and assigned to PP and pDA. In addition, two absorption bands at 1266 and 670 cm^{-1} specific for the LDH-RA hybrid system appeared.^[55,56] For LDH-EU-coated NWFs, the signal at 670 cm^{-1} was clearly visible and attributed to the crystal lattice vibration modes of LDHs. Additionally, an increase in the signal intensity in the region between 3700 and 3200 cm^{-1} due to the stretching of the hydroxyl groups of LDHs (which overlaps with the stretching of the -OH and -NH groups of the pDA) was observed for all samples.

These data confirmed the successful immobilization of the LDH-RA and LDH-EU on NWF and showed an increase in the

Table 3. TGA and OIT DSC data of NWF, NWF_P, NWF_pDA, NWF_P_pDA, and LDH-RA or LDH-EU surface NWF modified samples.

Sample	$T_{5\%}$ (°C) ^{a)}	T_{inf} (°C) ^{b)}	Residue (wt. %) ^{c)}	LDH content (wt. %) ^{d)}	OIT (min)
NWF	420 ± 3	468 ± 1	0.12 ± 0.09	–	1.7 ± 0.1
NWF_P	405 ± 9	469 ± 1	0.3 ± 0.1	–	<1
NWF_pDA	423 ± 4	468 ± 1	1.1 ± 0.6	–	9.8 ± 0.7
NWF_P_pDA	413 ± 3	473 ± 2	2.1 ± 0.4	–	1.5 ± 0.3
NWF_LDH-RA	419 ± 2	467 ± 1	1.0 ± 0.6	1.6 ± 0.9	6.3 ± 0.9
NWF_P_LDH-RA	402 ± 4	470 ± 1	1.9 ± 0.8	2.9 ± 1.4	<1
NWF_pDA_LDH-RA	420 ± 6	474 ± 2	2.8 ± 0.9	3.1 ± 0.9	19 ± 1
NWF_P_pDA_LDH-RA	405 ± 9	476 ± 1	3.9 ± 0.8	3.2 ± 0.7	1.6 ± 0.1
NWF_LDH-EU	420 ± 2	466 ± 1	0.8 ± 0.4	1.1 ± 0.5	13 ± 3
NWF_P_LDH-EU	398 ± 6	470 ± 4	2.9 ± 0.4	4.2 ± 0.6	1.8 ± 0.3
NWF_pDA_LDH-EU	418 ± 3	471 ± 2	2.8 ± 0.5	2.9 ± 0.5	15 ± 2
NWF_P_pDA_LDH-EU	400 ± 10	475 ± 4	4.1 ± 0.9	3.3 ± 0.7	2.0 ± 0.3

^{a)} Temperature corresponding to 5 wt.% loss; ^{b)} Temperature corresponding to the maximum degradation rate; ^{c)} Residue at 700 °C; ^{d)} This value was determined by comparing the % of residue at 700 °C with that of LDH-RA or LDH-EU and of the corresponding NWF (NWF or NWF_P or NWF_pDA or NWF_P_pDA).

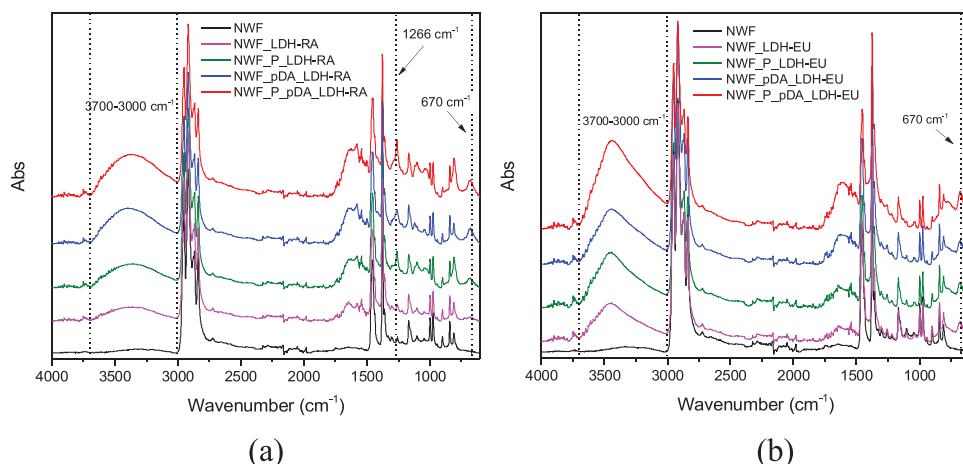


Figure 9. ATR FTIR of NWF, NWF_LDH-RA, NWF_P_LDH-RA, NWF_pDA_LDH-RA, NWF_P_pDA_LDH-RA a), and NWF_LDH-EU, NWF_P_LDH-EU, NWF_pDA_LDH-EU, NWF_P_pDA_LDH-EU b).

intensity of LDH-related signals for all plasma-treated and pDA-coated samples compared to the NWF_LDH-RA and NWF_LDH-EU samples. A detailed comparison of normalized spectra revealed that the combination of plasma and pDA treatments further increased the LDH content on the surface compared with pDA coating alone, consistently with a higher amount of pDA deposited after the combined treatment.

To further investigate the morphology of deposited LDH, SEM analysis was carried out on selected NWFs coated with LDH-RA and previously treated with plasma or pDA (**Figure 10**). SEM micrographs of NWF_P_LDH-RA (Figure 10a1-a3) showed a homogeneous distribution of the modified LDHs on the fiber surface, suggesting an almost complete coating. At higher magnifications, we observed some layered agglomerates with the typical structure of LDHs, varying in size from a few microns to a maximum of 2 μm . SEM micrographs of NWF_pDA_LDH-RA

(Figure 10b1-b3) showed numerous LDH particles deposited on the surface of fibers covered by pDA, retaining the desert rose structure typical of LDHs.

The thermal stability and LDH content of the samples were evaluated by TGA. The results showed that T_{inf} and $T_{5\%}$ values of PP fibers in LDH-RA and LDH-EU modified NWF samples were like those of the plasma-treated or pDA-coated samples, mainly influenced by the two functionalization treatments. Samples treated with plasma and then coated with LDH-RA or LDH-EU, indeed, continued to show lower $T_{5\%}$ compared to all other samples.

The residue value at 700 $^{\circ}\text{C}$ for all samples containing the modified LDHs was higher than those without them, as expected (Table 3). The amount of LDH deposited was estimated by comparing the residue at 700 $^{\circ}\text{C}$ for the LDH-coated samples with those of the hybrids analyzed under the same inert

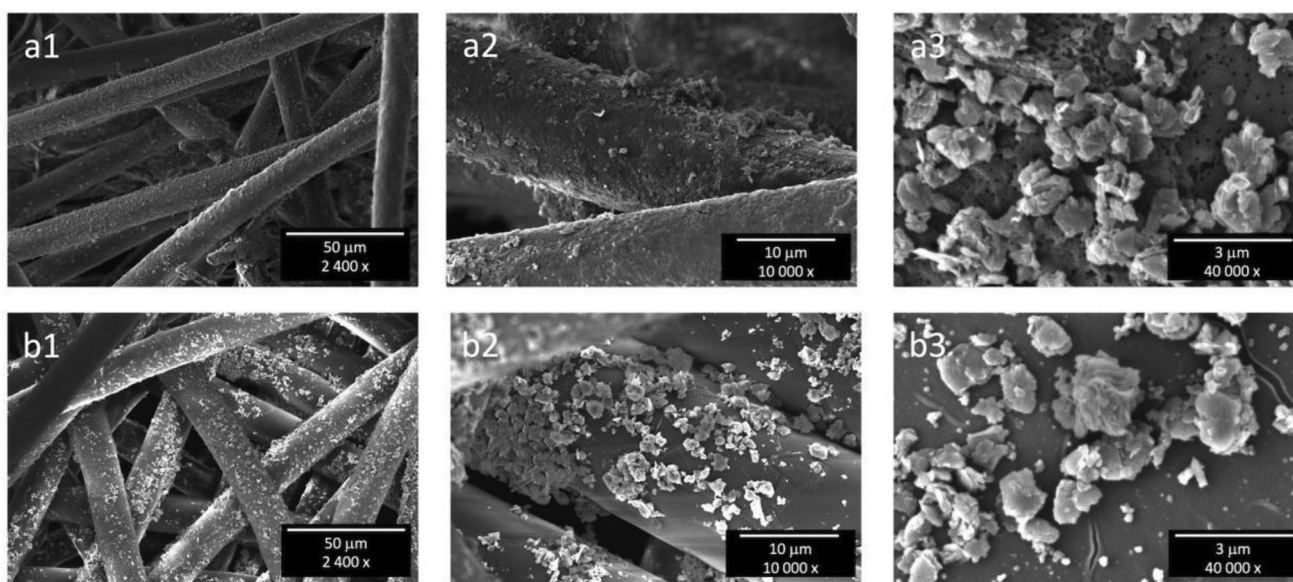


Figure 10. SEM micrographs at different magnifications of NWF_P_LDH-RA a1-a3) and NWF_pDA_LDH-RA b1-b3).

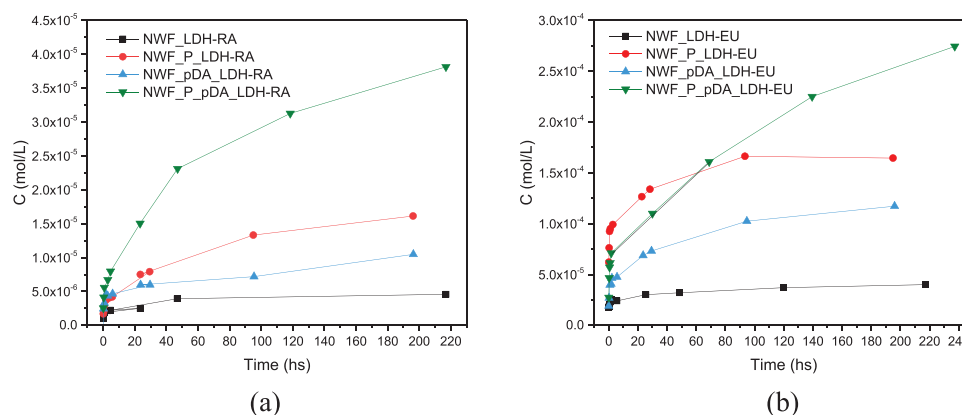


Figure 11. Concentration of RA and EU released at different times from LDH-RA-coated a) and LDH-EU-coated NWF samples b) in 95/5 H₂O/EtOH v/v solution.

conditions (Figure S8, Supporting Information), as well as with that of NWF, NWF_P, NWF_pDA, and NWF_P_pDA. The data confirmed that both pDA-coated and plasma-treated samples had a higher amount of LDHs retained on the surface compared to untreated samples (Figure S9, Supporting Information).

2.4. Antioxidant and Antimicrobial properties of LDH-coated Non-Woven-Fabrics

The antioxidant capacity of LDH-RA and LDH-EU deposited on NWF samples was assessed using the OIT test carried out with DSC. This test measures the sample's resistance to thermally induced oxidation by determining the time required for exothermic oxidation during an isothermal experiment performed under oxygen flow.^[16,24,57] The results gathered in Table 3 showed that NWF is oxidized at 180 °C in less than 2 min after introducing oxygen into the DSC chamber. Furthermore, the plasma treatment led to the production of oxidized species on the surface, which accelerated the degradation processes at high temperatures, reducing the substrate's OIT to less than 1 minute.

pDA-coated NWF exhibited instead a significantly higher OIT value, in an 8-min increment. This effect was attributed to the antioxidant properties of the catechol units in the pDA structure,^[58] which could capture free radicals formed during its degradation. However, the OIT value of NWF_P_pDA subjected to plasma treatment prior to pDA coating, was like that of NWF, indicating that pDA could help restore the thermal stability impaired by plasma treatment. The stability of NWF was enhanced by the modification with both LDH-RA and LDH-EU, but the LDH-EU system was found to provide greater thermo-oxidative stability compared to the LDH-RA system. This result matches the results of the DPPH analyses, and, as discussed above, may be attributed to the different morphology of the hybrids, which affects the availability of the active species. In the case of LDH-EU (i.e., LDH-EUsyn), the EU molecules were mainly adsorbed onto the surface of the LDH lamellae, whereas in the case of LDH-RA (i.e., LDH-RAsyn), the active molecules were intercalated and ionically bound. As a result, the EU molecules may be more easily available to protect the substrate as they migrate faster to the substrate. Besides, it is important to note that the

DPPH test was performed at room temperature, while the OIT test was carried out at high temperatures, which may impact the stability of the molecules and could therefore affect the results. The pre-treatment of the samples with plasma followed by coating with modified LDHs resulted in OIT values similar but still lower than those of the unmodified substrate, indicating partial recovery of the thermal stability of the starting samples. The coating with pDA and the subsequent deposition of LDH particles enhanced the stabilizing effects by promoting the increase in OIT values.

Migration tests were carried out for all the samples treated with modified LDHs to evaluate the migration ability of active molecules from hybrid systems deposited on NWF. Specifically, NWF samples were dipped in a hydroalcoholic solution (95/5 H₂O/EtOH v/v) for 10 days and the release of rosmarinic anion and eugenol was monitored by recording the UV-vis spectrum of the solution at different times. We compared the behavior of the samples treated with the two hybrids, LDH-RA and LDH-EU depending on the surface treatment. The results showed that unmodified NWF samples released concentrations of active molecules lower than surface-modified samples and quickly reached a plateau (Figure 11). However, the concentration of active molecules increased over time for all surface-modified NWFs due to their higher surface content of modified LDH, as confirmed by TGA analysis.

Between LDH-RA-coated and LDH-EU-coated NWF samples, the release rates of the active molecules varied depending on the surface treatment method and the amount of LDH-RA and LDH-EU retained.

In the case of LDH-RA-coated specimens, the samples treated with both plasma and pDA showed the highest release of rosmarinic anion over time, and the release was controlled and prolonged without reaching a *plateau*. Additionally, samples NWF_P_LDH-RA and NWF_pDA_LDH-RA showed similar release trends and concentrations, which correlated with the amount of LDH deposited on the surface, as determined by TGA.

In the case of LDH-EU-coated NWF samples, our results also demonstrated that the concentration of EU released was consistently higher than that released from NWF samples with deposited LDH-RA hybrid, regardless of the substrate pre-functionalization method employed. This finding can be

Table 4. Results of bactericidal test.

1 st set	<i>S. aureus</i> ^{a)} mean ± SD (CFU/mL)	Log 10 reduction	<i>P. aeruginosa</i> ^{b)} mean ± SD (CFU/mL)	Log 10 reduction
NWF	$8.40 \times 10^6 \pm 5.19 \times 10^6$	0	$5.65 \times 10^6 \pm 7.50 \times 10^6$	0
NWF_P_pDA_LDH-RA	$9.50 \times 10^5 \pm 3.15 \times 10^7$	0.94	$1.35 \times 10^6 \pm 7 \times 10^6$	0.62
2 nd set	<i>S. aureus</i> ^{c)} mean ± SD (CFU/mL)	Log 10 reduction	<i>P. aeruginosa</i> ^{d)} mean ± SD (CFU/mL)	Log 10 reduction
NWF_P_pDA	$3.2 \times 10^7 \pm 70$	0	$3.80 \times 10^5 \pm 95$	0
NWF_P_pDA_LDH-EU	$2.0 \times 10^5 \pm 10$	2.20	$1.30 \times 10^5 \pm 25$	0.47

^{a)} Initial titer of *S. aureus* in the 1st set was 1×10^8 CFU/mL; ^{b)} Initial titer of *P. aeruginosa* in the 1st set was 3×10^8 CFU/mL; ^{c)} Initial titer of *S. aureus* in the 2nd set was 4×10^7 CFU/mL; ^{d)} Initial titer of *P. aeruginosa* in the 2nd set was 3×10^7 CFU/mL. SD = standard deviation.

attributed to the fact that EU was mainly adsorbed onto LDH particles while RA was intercalated and ionically bound. Consequently, EU migrated faster from LDH-EU than RA from LDH-RA, resulting in a higher concentration of the released active molecule for the same amount of hybrid deposited on NWF.

The antimicrobial effectiveness of LDH-RA and LDH-EU was investigated through biological tests on selected samples: NWF_P_pDA_LDH-EU and NWF_P_pDA_LDH-RA. **Table 4** summarizes the results of bactericidal tests performed on *Staphylococcus aureus* and *Pseudomonas aeruginosa*.

NWF_P_pDA_LDH-EU revealed a significant bactericidal effect towards *S. aureus* with a 2.2 Log₁₀ reduction in bacterial growth compared to NWF_P_pDA, while its bactericidal activity against *P. aeruginosa* was lower, with an average of 0.47 Log₁₀ reduction. On the other hand, NWF_P_pDA_LDH-RA was less effective against *S. aureus*, with a 0.94 Log₁₀ reduction, compared to NWF, and showed similar bactericidal activity against *P. aeruginosa*, with a 0.62 Log₁₀ reduction. These results can be explained by the different bactericidal activity of EU and RA-H. Both biomolecules destroy bacterial membranes, which is their primary mechanism of action.^[59,60] RA-H is a hydrophobic molecule that can easily penetrate the lipopolysaccharide cell membrane and enter the cytoplasm. Studies have reported a greater efficacy of RA-H against gram-positive bacteria, which is consistent with our results showing higher bactericidal activity of NWF coated with LDH-RA particles against *S. aureus* than against *P. aeruginosa*.^[61–63]

Similarly, NWF_P_pDA_LDH-EU showed greater efficacy against *S. aureus* than *P. aeruginosa*, likely due to the different mechanisms of action of EU against the two bacterial strains. Molecular modeling studies have shown that EU reduces the transcription of the *pqsA* gene and influences the signal pathway of *P. aeruginosa* by decreasing the level of kynurenine. This effect can be reversed by the addition of exogenous kynurenine.^[64] Another study demonstrated that EU binds by hydrophobic interactions and hydrogen bonds to the critical amino acid residues Arg61 and Tyr41 of the LasR receptor, which play a role in biofilm formation. This decreases the ability of *P. aeruginosa* to form biofilm.^[65] EU's efficacy against gram-positive bacteria is attributed to the physical damage caused by the promoted production of reactive oxygen species that destroy the bacterial membrane, as demonstrated in previous studies.^[66]

These data demonstrate that both hybrids deposited on the substrate have a noteworthy antibacterial activity, although more work is needed to develop specific products.

3. Conclusion

Hybrid LDH systems with immobilized RA-H or EU have been successfully prepared using both commercial molecules and ethanolic extracts of sage and clove buds, which contain the target molecules. The extracts have been found to produce effective hybrid systems with features like those obtained using pure compounds. The two target molecules, which possess antimicrobial and antioxidant properties, have been transferred to the surface of PP NWF obtained from surgical masks coating the fibers with the LDH-based hybrid systems.

A significant increase in the amount of hybrid deposited was achieved when the NWF was first functionalized by plasma treatment, coated with pDA, or by a combination of both treatments. Notably, the combination of plasma and pDA resulted in the highest amount of functional hybrid retained on the substrate surface. The characterization studies have revealed that the type and concentration of hybrid influence the functional properties of NWF. Samples coated with LDH-EU have shown more effective antioxidant activity than those coated with LDH-RA, despite similar amounts being deposited. This difference has been attributed to the better migration capability of the EU, which is adsorbed in the LDH-EU hybrid and not intercalated like RA. A preliminary migration study in a hydroalcoholic environment has confirmed this result, as NWF_P_pDA_LDH-EU released a concentration of EU higher than its counterpart NWF_P_pDA_LDH-RA, which possessed a higher amount of LDH-RA on the surface. The NWF_P_pDA_LDH-EU sample exhibited significant antibacterial activity against *S. aureus*, likely due to the ability of EU to produce reactive oxygen species that can damage the bacterial membrane. The antibacterial effect of LDH-RA deposited on NWF was instead less specific towards both strains tested, and the bactericidal activity was lower. This may be attributed to the slower release of intercalated RA, potentially affecting its migration into the culture medium. This slower migration may hinder the molecule's ability to effectively reach and target the bacteria.

Overall, this study highlights the potential of LDHs as a versatile platform for immobilizing and controlling the release of bioactive molecules, which can be directly obtained from

agrifood extracts without any preliminary purification. The hybrids can provide enhanced thermal oxidation resistance and antimicrobial activity to NWF used in biomedical applications, which can be further improved by the pretreatment with cold plasma or coating with pDA. Both pretreatments, either individually or combined, were found to be effective in improving the adhesion and coating of NWF substrates with the hybrid particles, resulting in an increased content of bioactive molecules available on the NWF surface.

Among the prepared samples, LDH-EU has shown considerable promise in improving the thermal oxidation resistance and antimicrobial activity of NWF. Hence, NWF_P_pDA_LDH-EU could be further studied and developed into functional materials, extending its potential utility beyond healthcare applications.

4. Experimental Section

Materials: External spunbond layers of PP NWF surgical face masks, distributed in Italian schools during the COVID-19 pandemic, were cut into squares of approximately 5 cm on a side and used for modification and coating tests. Rosmarinic acid (RA-H, 96%, Sigma-Aldrich), eugenol (EU, 99%, Sigma-Aldrich), dopamine hydrochloride (DA, Sigma-Aldrich), tris(hydroxymethyl)aminomethane (TRIS, Carlo Erba), 2,2-diphenyl-1-picrylhydrazyl hydrate (DPPH, Sigma-Aldrich), ethanol (ACS reagent 96%, Sigma-Aldrich), acetone (ACS reagent $\geq 99.6\%$, Sigma-Aldrich), hexane ($\geq 99\%$, Sigma-Aldrich) and methanol (99+% extra pure, Acros Organics) were used as received. Magnesium aluminum hydroxy carbonate (LDH-CO₃) Pural MG63HT was provided by Sasol GmbH (Hamburg, Germany), and magnesium aluminum hydroxy nitrate (LDH-NO₃) was purchased from Prolabin & Tefarm (Perugia, Italy). Rosmarinic acid-modified LDH (LDH-RASyn and LDH-RAext) was synthesized from LDH-NO₃ according to the previous method.^[38,39] Dry clove buds were obtained from a local market, and sage leaves (*Salvia officinalis* L.) were collected from a plant located in Pisa (Italy). Deionized ultrapure water was produced using a Milli-Q system (Millipore, Bedford, MA, USA).

Extraction of Sage (*Salvia officinalis* L.) and Clove Buds: Sage leaves were freeze-dried using a Freeze-Dryer 5Pascal LIOSPDGT and subsequently pulverized with a laboratory blade mill. Approximately 25 g of the resulting powder was extracted using 170 mL of ethanol at 50 °C with magnetic stirring for 4 h. The suspension was then centrifugated at 5000 rpm for 15 min using an Eppendorf centrifuge model 5804R and the supernatant was dried using a rotavapor under reduced pressure. The resulting residue was then dried in a vacuum oven at 40 °C until a constant weight was achieved. Finally, liquid-liquid hexane-water extraction was performed to purify the dry extract and remove excess chlorophyll. The UV-vis analysis revealed that 1 g of sage powder contains about 20 mg of RA-H. Clove buds were pulverized with a laboratory blade mill, and approximately 5 g of powder was extracted using 50 mL of ethanol at room temperature with magnetic stirring for 24 h. The suspension was then centrifugated at 5000 rpm for 15 min, and the supernatant was dried using a rotavapor under reduced pressure. The resulting residue was dried in a vacuum oven at 40 °C until a constant weight was achieved. UV-vis analysis revealed that 1 g of clove bud powder contains approximately 150 mg of EU.

Preparation of LDH-EU: LDH-CO₃ was treated at 450 °C for 9 h in a muffle furnace to obtain the calcined form (CLDH). Synthetic EU (0.12 g) and clove extract were dissolved in EtOH/H₂O (1:3 vol/vol, 30 mL) previously degassed. Then CLDH (0.40 g) was added to the solution and the suspension was kept under nitrogen and at room temperature while stirring for 48 h. Finally, the powdered solid (LDH-EUsyn and LDH-EUext) was recovered by centrifugation, purified, and dried in a vacuum oven at 40 °C to constant weight (0.59 g).

Surface Functionalization of PP NWF with Oxygen-Plasma: PP NWF samples were surface activated using a plasma reactor (Tucano, Gambetti, Italy) with a chamber of about 5.5 L and a working area of 118 ×

310 mm². The samples were exposed to oxygen-plasma on both sides using selected parameters of time (5 min), power (150 W), and oxygen flow (15 sccm). PP NWF sample after plasma treatment was named NWF_P.

Coating of Polydopamine (pDA) on PP NWF: Dopamine solution was prepared by dissolving 0.2 g of dopamine (2 mg mL⁻¹) in 100 mL of Tris-HCl buffer (10 mM, pH 8.5). The liquor ratio of the PP NWF samples to the solution was 1:100. Dopamine self-polymerization was performed at room temperature with continuous stirring (80 rpm) for 24 h. Then, samples were taken out, rinsed several times with deionized water and methanol, and dried at 90 °C in an oven for 2 h. The procedure was carried out for both non-plasma-treated PP NWF (NWF) and plasma-treated PP NWF (NWF_P) samples. The pDA-coated samples were named NWF_pDA and NWF_P_pDA, respectively.

Deposition of LDH on NWF, NWF_P, NWF_pDA, NWF_P_pDA samples: In these experiments, it was employed LDH-RASyn and LDH-EUsyn hybrids, both of which were prepared using commercially available RA and EU. LDH coating on PP NWF samples (NWF, NWF_P, NWF_pDA, NWF_P_pDA) was achieved by first dispersing 100 mg of LDH-RASyn or LDH-EUsyn by ultrasonication using a Hielscher Ultrasonic Processor UP200St in 100 mL of water. Then, NWF samples were dipped in the LDH suspension for 72 h. The samples were washed with water and dried at 90 °C.

Characterization: Thermogravimetric analysis (TGA) experiments were collected on an SII ETG/DTA 7200 EXSTAR (Seiko instrument, Chiba, Japan). LDH samples (5–10 mg) were placed in alumina sample pans (70 μ L), and runs were carried out at the standard rate of 10 °C min⁻¹ from 30 to 900 °C under airflow (200 mL min⁻¹). In the case of NWF samples, samples (3–10 mg) were placed in alumina sample pans, and runs were carried out at the standard rate of 10 °C min⁻¹ from 30 to 700 °C under nitrogen (200 mL min⁻¹). All TGA experiments were recorded using the Muse Mobile Station software. TGA analyses were repeated three times per sample.

OIT measurements were performed using a differential scanning calorimeter DSC 4000 (Perkin-Elmer, Waltham, MA, USA) equipped with a 3-stage cooler able to reach -130 °C. The instrument was calibrated with indium (m.p. 156.6 °C, $\Delta H = 28.5$ J/g) and zinc (m.p. 419.5 °C). Measurements were performed on disk-shaped specimens with a weight of around 2–3 mg. Samples were isothermally treated at 30 °C under nitrogen flow (50 mL min⁻¹) for 5 min, then they were heated from 30 to 180 °C at 20 °C min⁻¹ under nitrogen flow (50 mL min⁻¹). After maintaining nitrogen for 5 min to obtain thermal equilibrium, the gas was switched to oxygen flow (50 mL min⁻¹). The OIT was determined from the onset of the exothermic oxidation reaction of PP shown in the calorimetric curves. Three determinations were done for each sample and the OIT average value was reported.

XRD analysis has been performed at room temperature with an X'Pert PRO (PANalytical) powder diffractometer using Ni-filtered Cu K α radiation (1.541874 Å). All spectra were acquired at room temperature using a Si wafer as a zero-background sample holder in the 2 θ range between 1.5 and 30°, applying a step size of 0.0131° and a counting time per step of 208 s. The basal spacing of LDHs d(003) was calculated by applying Bragg's law.

Attenuated total reflectance (ATR) Fourier Transform Infrared (FTIR) spectra were recorded at room temperature with a Perkin-Elmer Spectrum Two spectrometer equipped with the ATR accessory with diamond crystal. The spectra were acquired in the 4000–650 cm⁻¹ region with a resolution of 4 cm⁻¹ using 16 scans. The spectra of LDHs and of the organic molecules were carried out in transmittance mode in the 4000–450 cm⁻¹ region with a resolution of 4 cm⁻¹ using 16 scans by mixing the samples with potassium bromide. For each sample 16 scans were recorded, averaged, and Fourier-transformed to produce a spectrum with a nominal resolution of 4 cm⁻¹.

UV-vis absorption spectra were recorded at room temperature with a Jasco V-750 UV-visible spectrophotometer (Jasco International Co. Ltd., Tokyo, Japan). Calibration curves of RA-H and EU were obtained by recording the absorbance of solutions of each molecule at different concentrations and by performing a linear fitting of the absorbance as a function of the molar concentration of the molecules (Figure S1, Supporting Information). The absorbance was recorded at the maximum wavelength for

each molecule, which was 330 nm for RA-H and 280 nm for EU. The following molar extinction coefficients were calculated: RA-H $\epsilon_{330} = 18500 \text{ M}^{-1} \text{ cm}^{-1}$ and EU $\epsilon_{260} = 10800 \text{ M}^{-1} \text{ cm}^{-1}$. The amount of RA-H and EU in the modified LDHs was determined by dissolving a known quantity (2-3 mg) of each LDH in concentrated HCl (a few drops), and then diluting the solution with EtOH until an absorbance lower than 1 was obtained. UV-vis spectra were recorded from the resulting solutions, and based on previously reported molar extinction coefficients, the quantity of the organophilic fraction was determined.

Scanning electron microscopy analyses were carried out at the “Centro per l’Integrazione della Strumentazione Scientifica – Università di Pisa (CISUP)” using a FEI Quanta 450 FEG-SEM equipped with an EDX spectrometer Bruker QUANTAX XFlash Detector 6|10. The micrographs were recorded on the surface of NWF samples before and after treatments. In order to increase their conductivity, all samples were covered with platinum before SEM observations with a high vacuum sputter and C-thread coater Leica EM ACE600.

DPPH Assay: The radical scavenging activity of RA-H, EU, LDH-RA_{syn}, LDH-RA_{ext}, LDH-EU_{syn}, and LDH-EU_{ext} was evaluated using the DPPH method. Stock solutions of DPPH ($6.15 \times 10^{-5} \text{ M}$), RA-H, EU, and suspensions of LDH-RA and LDH-EU with a concentration of active molecules of $6.15 \times 10^{-4} \text{ M}$ were prepared. The LDH suspensions were sonicated for 10 min using a Hielscher Ultrasonic Processor UP200St to enhance the delamination of the organophilic LDH. Next, 980 μL of the DPPH solution was mixed with 20 μL of RA-H and EU solutions or 20 μL of LDH-RA and LDH-EU suspensions.

All solutions/suspensions were kept in the dark and UV-vis spectra were recorded after 30 min and 24 h. The antioxidant activity of the samples was determined by calculating the percentage of quenched DPPH using the following formula:

$$\% \text{DPPH}_{\text{quenched}} = \left[1 - \left(\frac{A_s - A_b}{A_c - A_b} \right) \right] \times 100 \quad (1)$$

where A_s is the absorbance of the DPPH solution in the presence of the antioxidant. The A_s absorbance was obtained by adding 980 μL of the DPPH solution to 20 μL of the sample solution; A_b is the absorbance of the solvent used to prepare the DPPH solution; A_c is the absorbance of the control sample (i.e., 980 μL of the DPPH solution plus 20 μL of methanol).

Migration Test: Migration tests of rosmarinate anions (RA) and EU from LDH-modified NWF were carried out by soaking 25 mg sample in 5 mL of EtOH/H₂O 95/5 (v/v) at room temperature under stirring at 300 rpm. The release kinetics of rosmarinate anion and EU were followed by UV-vis spectroscopy by recording UV-vis spectra of solutions at different time points.

Antibacterial Test: To evaluate the antimicrobial efficacy of LDH-RA and LDH-EU, two experiments were set up according to ISO 20743:2021. The microorganisms used in all assays were *Staphylococcus aureus* (ATCC 25923) and *Pseudomonas aeruginosa* (ATCC 10145). In the first experiment the tested materials were untreated NWF and NWF_P_pDA_LDH-RA, while in the second one, the tested materials were NWF_P_pDA and NWF_P_pDA_LDH-EU.

Three coupons (10 mm X 10 mm) were tested for each material and for each strain. Briefly, the coupons were sterilized before the test (in autoclave). Test inoculum for each bacterial strain was prepared to a concentration of 10^8 CFU/mL by McFarland’s nephelometer. 10 μL of each bacterial strain suspension was deposited on each tested material. The coupons were dried in a biological safety cabinet class 2. Once dried, each coupon was placed in sterile jars containing 10 mL of SCDLP medium (peptone digest of casein 17 g; peptone digest of soybean 3 g; sodium chloride (NaCl) 5 g; dipotassium hydrogenphosphate 2,5 g; glucose 2,5 g; lecithin 1 g; polysorbate80 7 g and water 1000 mL) gently stirred for 20 min to ensure proper mixing. At the end of the incubation, serial dilutions were done for each solution and subsequently plated on Plate Count Agar (PCA, VWR International PBI, Radnor, PA, USA) and incubated for 18 to 24 h at $36 \pm 1 \text{ }^\circ\text{C}$ to determine the titer of the remanent viable bacteria after the contact time. Descriptive statistics of empirical data were calculated as mean of base-10 logarithmic (log 10) CFU reduction together with 95% confi-

dence intervals, to evaluate the reliability of measurements. ISO 20743 was required for the reduction of at least 4 Log 10 between untreated and treated textile product for the determination of the antimicrobial activity. The formula below was applied for the calculation of antimicrobial activity:

$$A = (\log 10C_t - \log 10C_0) - (\log 10T_t - \log 10T_0) = F - G \quad (2)$$

where A is the antibacterial activity value; F is the growth value on the control specimen; G is the growth value on the antibacterial testing specimen; $\log 10C_t$ is the logarithm of the arithmetic average of the numbers of bacteria obtained from $N = 3$ test control specimens after 18 to 24 h incubation; $\log 10C_0$ is the logarithm of the arithmetic average of the numbers of bacteria obtained from $N = 3$ control specimens immediately after inoculation (0 contact time); $\log 10T_t$ is the logarithm of the arithmetic average of the numbers of bacteria obtained from $N = 3$ antibacterial testing specimens after 18 to 24 h incubation; $\log 10T_0$ is the logarithm of arithmetic average of the numbers of bacteria obtained from $N = 3$ antibacterial testing specimens immediately after inoculation.

Supporting Information

Supporting Information is available from the Wiley Online Library or from the author.

Acknowledgements

This study was partially carried out within the MICS (Made in Italy – Circular and Sustainable) Extended Partnership and received partial funding from the European Union Next-GenerationEU (PIANO NAZIONALE DI RIPRESA E RESILIENZA (PNRR) – MISSIONE 4 COMPONENTE 2, INVESTIMENTO 1.3 – D.D. 1551.11-10-2022, PE00000004). This manuscript reflects only the authors’ view and opinion, neither the European Union nor the European Commission can be considered responsible for them.

Open Access Funding provided by Consiglio Nazionale delle Ricerche within the CRUI-CARE Agreement.

The open access funding statement was added on December 5, 2023, after initial online publication.

Conflict of Interest

The authors declare no conflict of interest.

Data Availability Statement

The data that support the findings of this study are available in the supplementary material of this article.

Keywords

layered double hydroxides, phenolic compounds, plasma, polydopamine, polypropylene non-woven fabric

Received: May 18, 2023
Revised: September 15, 2023
Published online: October 18, 2023

- [1] H. A. Maddah, *Am. J. Polym. Sci.* **2016**, 6, 1.
- [2] L. R. Crilly, A. A. Angelucci, B. Malile, C. J. Young, T. C. VandenBoer, J. I. L. Chen, *Environ. Sci.: Nano* **2021**, 8, 1603.
- [3] T. S. Muzata, A. Gebrekrestos, S. S. Ray, *ACS Omega* **2021**, 6, 28463.
- [4] A. Tuñón-Molina, K. Takayama, E. M. Redwan, V. N. Uversky, J. Andrés, Á. Serrano-Aroca, *ACS Appl. Mater. Interfaces* **2021**, 13, 56725.

- [5] W. C. Lu, C. Y. Chen, C. J. Cho, M. Venkatesan, W. H. Chiang, Y. Y. Yu, C. H. Lee, R. H. Lee, S. P. Rwei, C. C. Kuo, *Polymers* **2021**, *13*, 1122.
- [6] A. Tuñón-Molina, A. Cano-Vicent, M. Martí, Y. Muramoto, T. Noda, K. Takayama, Á. Serrano-Aroca, *bioRxiv* **2021**, 456330.
- [7] E. Faure, C. Falentin-Daudré, C. Jérôme, J. Lyskawa, D. Fournier, P. Woisel, C. Detrembleur, *Prog. Polym. Sci.* **2013**, *38*, 236.
- [8] J. Brito, H. Hlushko, A. Abbott, A. Aliakseyeu, R. Hlushko, S. A. Sukhishvili, *ACS Appl. Mater. Interfaces* **2021**, *13*, 41372.
- [9] M. F. Montenegro-Landívar, P. Tapia-Quirós, X. Vecino, M. Reig, C. Valderrama, M. Granados, J. L. Cortina, J. Saurina, *Sci. Total Environ.* **2021**, *801*, 149719.
- [10] N. Oulahal, P. Degraeve, *Front Microbiol* **2022**, *12*, 3906.
- [11] K. Khwaldia, N. Attour, J. Matthes, L. Beck, M. Schmid, *Compr Rev Food Sci Food Saf* **2022**, *21*, 1218.
- [12] C. M. Yang, K. Chathuranga, J. S. Lee, W. H. Park, *Polym. Test.* **2022**, *116*, 107786.
- [13] J. Andrade, C. González-Martínez, A. Chiralt, *Food Packag. Shelf Life* **2022**, *33*, 100855.
- [14] D. J. da Silva, M. M. de Oliveira, S. H. Wang, D. J. Carastan, D. S. Rosa, *Food Packag. Shelf Life* **2022**, *34*, 100929.
- [15] M. Ramos, A. Jiménez, M. Peltzer, M. C. Garrigós, *J Food Eng* **2012**, *109*, 513.
- [16] E. Passaglia, B. Campanella, S. Coiai, F. Cicogna, A. Carducci, M. Verani, I. Federigi, B. Casini, B. Tuvo, E. Bramanti, *ChemistrySelect* **2021**, *6*, 2288.
- [17] I. Volf, I. Ignat, M. Neamtu, V. I. Popa, *Chem. Pap.* **2014**, *68*, 121.
- [18] R. Morent, N. de Geyter, C. Leys, L. Gengembre, E. Payen, *Surf Interface Anal* **2008**, *40*, 597.
- [19] L. Carrino, G. Moroni, W. Polini, *J. Mater. Process. Technol.* **2002**, *121*, 373.
- [20] E. Bormashenko, G. Whyman, V. Multanen, E. Shulzinger, G. Chaniel, *J. Colloid Interface Sci.* **2015**, *448*, 175.
- [21] N. Gomathi, R. Rajasekar, R. R. Babu, D. Mishra, S. Neogi, *Mater. Sci. Eng. C* **2012**, *32*, 1767.
- [22] D. Moradi, Y. Ramezan, S. Eskandari, H. Mirsaeedghazi, M. J. Dakheli, *Food Packag. Shelf Life* **2023**, *35*, 101012.
- [23] S. Habib, M. Lehocky, D. Vesela, P. Humpolíček, I. Krupa, A. Popelka, *Polymers* **2019**, *11*, 1704.
- [24] F. Cicogna, E. Bramanti, B. Campanella, S. Caporali, L. Panariello, C. Cristallini, R. Ishak, N. Barbani, E. Passaglia, S. Coiai, *Molecules* **2022**, *27*, 8632.
- [25] H. Feinberg, T. W. Hanks, *Polym. Int.* **2022**, *71*, 578.
- [26] K. Y. Ju, Y. Lee, S. Lee, S. B. Park, J. K. Lee, *Biomacromolecules* **2011**, *12*, 625.
- [27] K. G. Malollari, P. Delparastan, C. Sobek, S. J. Vachhani, T. D. Fink, R. H. Zha, P. B. Messersmith, *ACS Appl. Mater. Interfaces* **2019**, *11*, 43599.
- [28] X. Saitaer, N. Sanbhal, Y. Qiao, Y. Li, J. Gao, G. Brochu, R. Guidoin, A. Khatri, L. Wang, *Coatings* **2019**, *9*, 164.
- [29] W. Zhou, W. Zhang, Z. Chen, *Appl. Surf. Sci.* **2017**, *392*, 153.
- [30] V. K. Thakur, D. Vennerberg, M. R. Kessler, *ACS Appl. Mater. Interfaces* **2014**, *6*, 9349.
- [31] H. Andishmand, S. Azadmard-damirchi, H. Hamishekar, M. A. Torbati, M. S. Kharazmi, G. P. Savage, C. Tan, S. M. Jafari, *Adv. Colloid Interface Sci.* **2023**, *311*, 102833.
- [32] S. Coiai, B. Campanella, R. Paulert, F. Cicogna, E. Bramanti, A. Lazzari, L. Pistelli, M. B. Coltelli, *Appl. Sci.* **2021**, *11*, 9249.
- [33] S. Kesavan Pillai, P. Kleyi, M. de Beer, P. Mudaly, *Appl. Clay Sci.* **2020**, *199*, 105868.
- [34] E. Boccalon, G. Gorrasi, M. Nocchetti, *Adv. Colloid Interface Sci.* **2020**, *285*, 102284.
- [35] M. Bastianini, C. Faffa, M. Sisani, A. Petracci, *Cosmetics* **2018**, *5*, 51.
- [36] C. Rossi, A. Schoubben, M. Ricci, L. Perioli, V. Ambrogio, L. Latterini, G. G. Aloisi, A. Rossi, *Int. J. Pharm.* **2005**, *295*, 47.
- [37] H. Kang, H. J. Kim, J. H. Yang, T. H. Kim, G. Choi, S. M. Paek, A. J. Choi, J. H. Choy, J. M. Oh, *Appl. Clay Sci.* **2015**, *112–113*, 32.
- [38] S. Coiai, F. Cicogna, S. Pinna, R. Spiniello, M. Onor, W. Oberhauser, M. B. Coltelli, E. Passaglia, *Appl. Clay Sci.* **2021**, *214*, 106276.
- [39] F. Cicogna, E. Passaglia, M. Benedettini, W. Oberhauser, R. Ishak, F. Signori, S. Coiai, *Molecules* **2023**, *28*, 347.
- [40] A. Megalathan, S. Kumarage, A. Dilhari, M. M. Weerasekera, S. Samarasinghe, N. Kottegoda, *Chem. Cent. J.* **2016**, *10*, 35.
- [41] L. Sisti, G. Totaro, A. Celli, A. Diouf-Lewis, V. Verney, F. Leroux, *J. Environ. Chem. Eng.* **2019**, *7*, 103026.
- [42] L. Sisti, G. Totaro, N. Bozzi Cionci, D. di Gioia, A. Celli, V. Verney, F. Leroux, *Int. J. Mol. Sci.* **2019**, *20*, 2376.
- [43] J. Kerosenewala, P. Vaidya, V. Ozarkar, Y. Shirapure, A. P. More, *Polym. Bull.* **2022**, *80*, 7047.
- [44] A. S. Marchev, L. v. Vasileva, K. M. Amirova, M. S. Savova, I. K. Koycheva, Z. P. Balcheva-Sivenova, S. M. Vasileva, M. I. Georgiev, *Trends Food Sci. Technol.* **2021**, *117*, 182.
- [45] R. S. Pizani, J. Viganó, L. M. de Souza Mesquita, L. S. Contieri, V. L. Sanches, J. O. Chaves, M. C. Souza, L. C. da Silva, M. A. Rostagno, *Trends Food Sci. Technol.* **2022**, *127*, 245.
- [46] M. X. Zhu, Y. P. Li, M. Xie, H. Z. Xin, *J Hazard Mater* **2005**, *120*, 163.
- [47] S. Coiai, S. Javarone, F. Cicogna, W. Oberhauser, M. Onor, A. Pucci, P. Minei, G. Iasilli, E. Passaglia, *Eur. Polym. J.* **2018**, *99*, 189.
- [48] A. Joardar, G. Meher, B. P. Bag, H. Chakraborty, *J. Mol. Liq.* **2020**, *319*, 114336.
- [49] J. Gonzalez-Rivera, C. Duce, B. Campanella, L. Bernazzani, C. Ferrari, E. Tanzini, M. Onor, I. Longo, J. C. Ruiz, M. R. Tinè, E. Bramanti, *Ind. Crops Prod.* **2021**, *161*, 113203.
- [50] K. Mishra, H. Ojha, N. K. Chaudhury, *Food Chem.* **2012**, *130*, 1036.
- [51] Z. Cheng, J. Moore, L. Yu, *J. Agric. Food Chem.* **2006**, *54*, 7429.
- [52] R. A. Zangmeister, T. A. Morris, M. J. Tarlov, *Langmuir* **2013**, *29*, 8619.
- [53] S. Liu, Y. Chen, C. Liu, L. Gan, X. Ma, J. Huang, *Cellulose* **2019**, *26*, 9599.
- [54] L. Zhu, Y. Lu, Y. Wang, L. Zhang, W. Wang, *Appl. Surf. Sci.* **2012**, *258*, 5387.
- [55] K. Stehfest, M. Boese, G. Kerns, A. Piry, C. Wilhelm, *J. Plant Physiol.* **2004**, *161*, 151.
- [56] R. Swisłocka, E. Regulska, J. Karpinska, G. Swiderski, W. Lewandowski, *Molecules* **2019**, *24*, 2645.
- [57] L. P. Amaro, F. Cicogna, E. Passaglia, E. Morici, W. Oberhauser, S. Al-Malaika, N. T. Dintcheva, S. Coiai, *Polym. Degrad. Stab.* **2016**, *133*, 92.
- [58] F. Mollica, R. Lucernati, R. Amorati, *J. Mater. Chem. B* **2021**, *9*, 9980.
- [59] D.-P. Hu, J.-R. Zhao, Y.-Z. Gu, H.-X. Xu, X.-Q. Li, *Lat. Am. J. Pharm.* **2015**, *34*, 1866.
- [60] M. Ulanowska, B. Olas, *Int. J. Mol. Sci.* **2021**, *22*, 3671.
- [61] T. Mencherini, P. Picerno, C. Scesa, R. Aquino, *J. Nat. Prod.* **2007**, *70*, 1889.
- [62] A. Klančnik, S. Piskernik, B. Jeršek, S. S. Možina, *J Microbiol Methods* **2010**, *81*, 121.
- [63] L. Slobodníková, S. Fialová, H. Hupková, D. Grančai, *Nat. Prod. Commun.* **2013**, *8*, 1934578X1300801223.
- [64] J. H. A. Omanakuttan, N. Pandurangan, V. S. Vargis, M. Maneesh, B. G. Nair, G. B. Kumar, *Appl. Microbiol. Biotechnol.* **2016**, *100*, 3681.
- [65] Y. G. Kim, J. H. Lee, S. Il Kim, K. H. Baek, J. Lee, *Int. J. Food Microbiol.* **2015**, *195*, 30.
- [66] B. Das, D. Mandal, S. K. Dash, S. Chattopadhyay, S. Tripathy, D. P. Dolai, S. K. Dey, S. Roy, *Infect. Dis.: Res. Treat.* **2016**, *9*, IDRTS31741.